

Research papers

Identification of hydroclimate subregions for seasonal drought monitoring in the U.S. Great Plains



Zachary T. Zambreski^{a,*}, Xiaomao Lin^a, Robert M. Aiken^b, Gerard J. Kluitenberg^a,
Roger A. Pielke Sr^c

^a Department of Agronomy, Kansas State University, Throckmorton Hall, Plant Sciences Center, Manhattan, KS 66506, USA

^b Department of Agronomy, Kansas State University, Northwest Research–Extension Center, Colby, KS 67701, USA

^c Department Atmospheric and Oceanic Sciences, and Cooperative Institute for Research in Environmental Sciences, University of Colorado at Boulder, CO 80309, USA

ARTICLE INFO

This manuscript was handled by Andras Bardossy, Editor-in-Chief, with the assistance of Vazken Andréassian, Associate Editor

Keywords:

Drought
Empirical orthogonal functions
Climate
Agriculture
SPEI

ABSTRACT

Identification of subregions that share similar historical drought variability provides useful information for drought monitoring, mitigation planning, and resource allocation. This study examined space-time historical drought variability for the Great Plains spanning from 1901 to 2015 by using rotated Empirical Orthogonal Functions (rEOFs). The Standardized Precipitation-Evapotranspiration Index (SPEI) on a three-month timescale was utilized to examine spatial and temporal changes in agricultural drought. We propose a new procedure for identifying the number of rEOFs to be selected for reconstructing subregions. Drought event intensities of moderate, severe, and extreme categories increased in recent years although the number of drought events decreased. Seasonal rEOFs demonstrated that 9–12 subregions were adequate to explain a significant proportion of the original variability in the Great Plains. The time series for each subregion was highly correlated to the original SPEI data and reflected the seasonal meteorological processes that drive drought variability. Several significant wetting trends were found, and there was statistical evidence that drought and wetting event severities had increased for a few subregions. Summer drought has become more variable across space and time, indicating that a more diverse set of resources and strategies might be needed to mitigate impacts of spatially-variable drought and wetting events in coming decades. Winter season drought has become less variable, indicating that perhaps resources could be consolidated when dealing with impacts on a larger scale; however, less variability implies that drought and wetting events may occur across larger regions of the Great Plains during a given season.

1. Introduction

Regionalizing variability across space and time is a complex multi-scalar problem. The demand for regional assessments of historical climate variability is growing due to its value in decision-making processes such as the management of water resources and agricultural systems (Bonaccorso et al., 2003; Omondi et al., 2013). The Great Plains of the United States is a significant contributor to U.S. and global food production and relies on both optimal climatic conditions and crop management practices to sustain high production. Changes in regional climate due to human and natural variations and long-term change generate uncertainty in global food security (Easterling et al., 1993; Pielke et al., 2013). Daily, monthly, and annual perturbations in weather and climate across this agricultural region create significant impacts at local and regional scales. Drought, a condition of moisture

deficit sufficient to have an adverse effect on vegetation, animals, and society, is a multi-faceted and complex climate-related phenomenon (Sönmez et al., 2005; Warwick, 1975). The Great Plains has experienced highly variable drought conditions throughout the historical climate record (since the late 1800s). The most notable droughts include the multi-year droughts of the 1930s and 1950s and the more recent droughts in the late 1980s and 2011–2012 that resulted in billions of dollars in agricultural losses (Svoboda et al., 2002). Human activity such as the expansion of agriculture into marginal lands (Colaizzi et al., 2009) or groundwater depletion (Russo and Lall, 2017) has been shown to modify the vulnerability of agricultural systems to drought impacts. Poor management practices during the Dust Bowl era of the 1930s led to high rates of soil erosion and decreasing land productivity that resulted in off-farm migration (McLeman et al., 2014). Changes in policy and management practices that resulted from lessons

* Corresponding author at: 1712 Claflin Road, 2718 Throckmorton PSC, Manhattan, KS 66506, USA.

E-mail address: ztz@ksu.edu (Z.T. Zambreski).

learned during the 1930s resulted in less severe agricultural impacts during the 1950s (Wiener et al., 2016). Rising temperatures would intensify droughts due to increases in evaporation from the soil and transpiration from vegetation leading to more frequent withdrawals of underground water resources (IPCC, 2014). Across the Great Plains, such a change would increase the number of climate-related challenges and might include (1) resolving increasing competition among land, water, and energy resources; (2) developing sustainable agricultural systems; (3) conserving diverse ecological systems; and (4) enhancing the resilience of communities to the impacts of extreme events, including more intense heat waves, cold snaps, drought, and flooding events (Shafer et al., 2014).

The Great Plains cover a wide range in latitude and elevation, spanning the continental land area between northern Mexico and the Prairie provinces of Canada and experiencing an elevation gain of more than a thousand meters from Texas to the base of the Rocky Mountains. Although its latitudinal extent exceeds its spread in longitude, the Great Plains has a gradient in annual precipitation of more than 1200 mm in gulf coastal areas in the southeast to less than 400 mm at the eastern slopes of the Rocky Mountains (Pielke and Doesken, 2008). The Köppen climate classification divides the Great Plains into four main categories: humid subtropical, hot-summer humid continental, warm-summer humid continental, and cold semi-arid (Köppen, 2011). Differences in classifications are generally driven by latitude and elevation, corresponding with gradients in annual mean temperature and precipitation. The precipitation gradient results in two types of grasslands that dominate the Great Plains: short and tallgrass prairie in the west and east, respectively (Küchler, 1964). These grasslands are vital ecosystems for farming, grazing, and biofuel production and are highly sensitive to rainfall variability (Knapp and Smith, 2001; Shafer et al., 2014). Low precipitation during the growing season can trigger agricultural drought, which occurs when soil moisture availability falls below a level that has an adverse effect on crop production (Panu and Sharma, 2002). The economic importance of this region and the space-time variability of precipitation and temperature underscore the need for additional assessments of drought variability on timescales affecting these agricultural and socioeconomic systems, e.g., seasonal and monthly.

Several studies and methods have been used to examine historical drought variability of the Great Plains. Although records of climate observations began in the late 1800s, scientists have used tree rings to reconstruct the paleoclimatic record over the last several centuries, indicating that multi-decadal droughts as severe as major droughts of the twentieth century have occurred in the Great Plains in the last millennium (Sauchyn et al., 2003; Stockton and Meko, 1983; Woodhouse and Overpeck, 1998). Other methods have been utilized to examine the characteristics of drought during the instrumental record. Guttman (1998) used spectral analysis of several drought indices to classify weather stations across the United States according to their characteristics, and his results demonstrated incoherent regional patterns in the Great Plains. Other studies have used the trends directly calculated from the Standardized Precipitation Index (SPI) or the Palmer Drought Severity Index (PDSI) to show both wetting and drying has occurred across areas of the Great Plains (Logan et al., 2010; Yuan and Quiring, 2014). In addition to drought indices, land surface modeling has been utilized to study the mechanisms that drive soil moisture deficits in the Great Plains, showing that antecedent moisture conditions can have an impact on drought severity during the summer growing season (Livneh and Hoerling, 2016). Broader studies of drought trends over the contiguous United States show a decrease in the percentage of dry areas from the 1950s to 1990s and an increase in the percentage of dry areas since the 1990s (Dai, 2011). These studies demonstrate that regional variations in drought exist, and characterizing large areas such as the Great Plains as a single region can produce misleading drought metrics that are not representative of the unique subregions that may exist. Emerging techniques provide an opportunity

to more accurately identify and characterize the spatio-temporal structures of regional historical drought variability.

Empirical Orthogonal Function (EOF) analysis, a multivariate statistical method first used for climatological applications in the 1950s (Lorenz, 1956), has been utilized in diverse applications to analyze the spatial and temporal variability of geophysical datasets (Bjornsson and Venegas, 1997). The EOF procedure constructs orthogonal linear combinations that explain the maximum amount of variance in both space and time. Through various rotations of these linear combinations, geographic regions of similar variability can be identified. Karl and Koscielny (1982) used EOF analysis to regionalize drought across the United States from long-term records of PDSI. Nine broad regions were identified, and spectral analysis revealed that regions in the interior U.S. experienced longer duration droughts. Other large- and small-scale studies of drought EOFs have been conducted across the globe in regions including China (Cai et al., 2015), Romania (Bojariu et al., 2012; Cheval et al., 2014), Portugal (Martins et al., 2012; Santos et al., 2010), the Iberian Peninsula (Vicente-Serrano, 2006), Turkey (Tatli and Türkeş, 2011), and Sicily (Bonaccorso et al., 2003). For example, Raziei et al., (2010) regionalized drought across Iran into four subregions based on the variability of the SPI at a time scale of 24 months. In these studies, applications of EOF analysis included but were not limited to (1) assessment of the similarities and differences amongst drought indices; (2) identification of strong and weak temporal signals in the drought time series; and (3) the separation of a region into sub-climate regimes. While many of these studies did not explore the drought metrics of these EOF indices such as duration, severity, or intensity, analysis of these metrics would enhance our understanding of the space-time variability of these intrinsic drought characteristics. Identifying regions that share similar drought variability is important for drought monitoring, drought mitigation planning, and drought emergency management. Given that sub-climates can span administrative regions, interagency cooperation could help improve drought preparedness. These insights are crucial for drought management agencies that require detailed but concise information on changes in historical climate for their areas.

The objective of this study was to investigate the spatial and temporal variability structures of seasonal and full-record monthly drought and wetting episodes in the Great Plains from 1901 to 2015 by identification of subregions from EOF analysis. We proposed a new EOF selection rule to identify significant subregions of variability. The Standardized Precipitation-Evapotranspiration Index (SPEI), a recently developed multi-scalar drought index that includes the effects of temperature variability, was chosen for this analysis as it can identify an increase in drought severity due to higher water demand as a result of evapotranspiration (Vicente-Serrano et al., 2010).

2. Material and methods

2.1. Study area and data source

For this study, the domain extended between latitudes $+32^\circ$ and $+48^\circ$ and longitudes -93° and -106° , covering over 2,100,000 km² of the central United States (Fig. 1). Monthly precipitation, temperature (maximum and minimum), and potential evapotranspiration coverage ($0.5^\circ \times 0.5^\circ$ grid) were obtained from the Climatic Research Unit TS v. 3.24.01 (CRU) at the University of East Anglia, UK (Harris et al., 2014) for years between 1901 and 2015. A total of 891 CRU grid points were used for the study. CRU was chosen for this analysis because its resolution allows for a reasonable number of grid points in the Great Plains to perform an EOF analysis. The inclusion of areas surrounding the Great Plains helps to avoid loss of variability and to isolate important drought features potentially hidden in a larger-scale analysis (Richman, 1986).

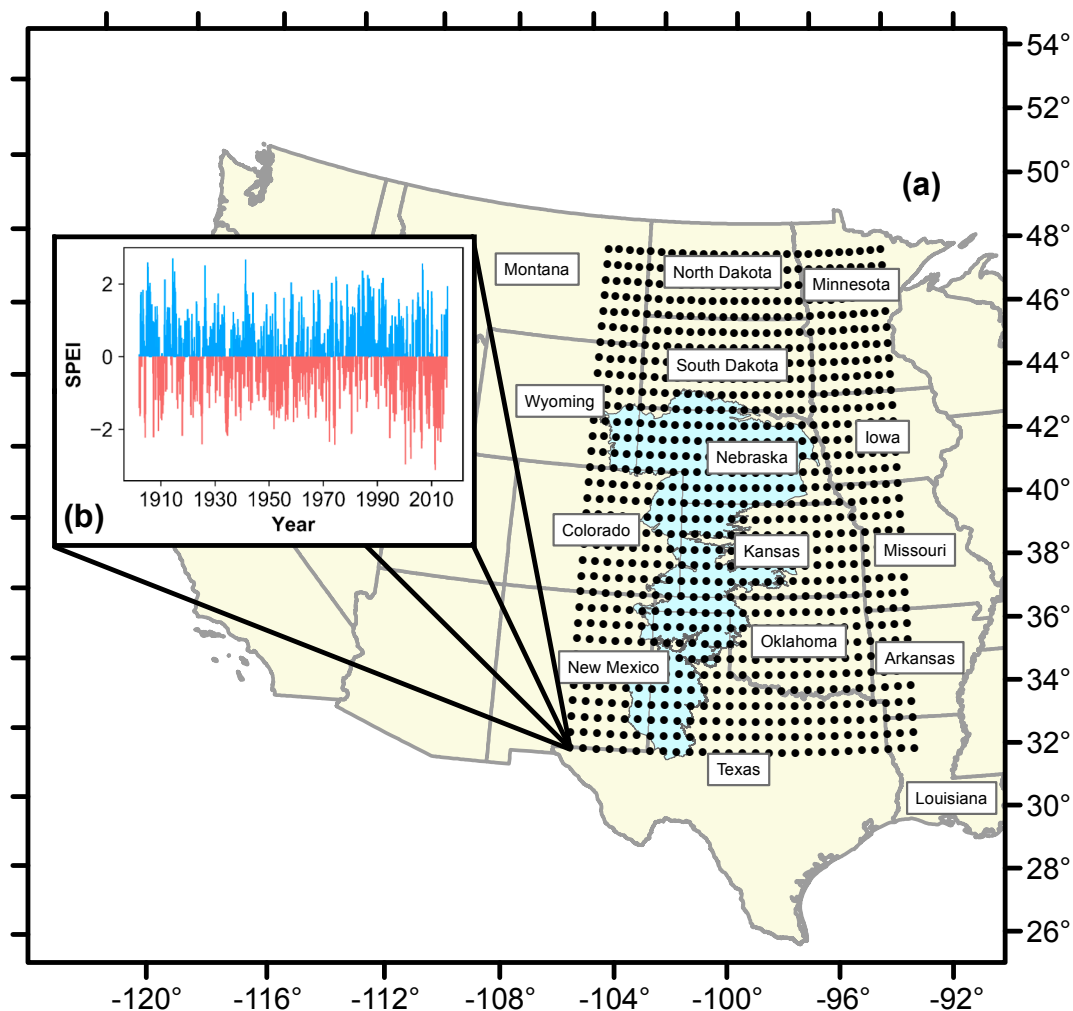


Fig. 1. (a) Study area of the U.S. Great Plains region and the Ogallala Aquifer (light blue) with black dots that illustrate selected grid points ($0.5^\circ \times 0.5^\circ$), and (b) Standardized Precipitation-Evapotranspiration Index (SPEI) for one grid point in the domain with dry (red) and wet (blue) events. (For interpretation of the references to color in this figure legend, the reader is referred to the web version of this article.)

2.2. Standardized precipitation-evapotranspiration index

Potential evapotranspiration (PE) provided by CRU was estimated using a variant of the Penman-Monteith procedure, and the difference between precipitation and PE is calculated for each month. These differences are summed based on the time scale chosen. Following the procedure in Vicente-Serrano et al. (2010), these summed differences are fitted to a three-parameter log-logistic cumulative probability distribution function, and this procedure is performed separately for each month and grid point. These probabilities are standardized using the approximation found in Zelan and Norman (1964) to obtain the SPEI. This index ranges in value from approximately -3 to approximately $+3$, with negative values indicating drier than normal conditions and positive values indicating conditions wetter than normal. SPEI values less than -2.0 or greater than 2.0 are considered extreme. Time series of SPEI values were calculated using tools developed at Kansas State University. The index was calibrated using data from the period 1931–1990. A time scale of three months was used to represent short-term drought which is more closely related to agricultural drought (Vicente-Serrano et al., 2011). The earliest available 3-month SPEI was March 1901. The model fit between observed summed differences of precipitation and PE and the expected values from the fitted log-logistic distribution was evaluated for each month using the Kolmogorov-Smirnov test at each grid point. No test resulted in rejection of the null hypothesis that the data come from the log-logistic distribution,

indicating that the statistical assumptions behind the SPEI are valid for this region.

2.3. Drought metrics

Duration, severity, and intensity were used to characterize drought and wetting events in each time series of SPEI values. The duration of a drought event is the length of time (in months) that the drought index is consecutively at or below a given truncation threshold. Similarly, the duration of a wetting event is the length of time (in months) that the drought index is at or above a given threshold. The severity of each event is the cumulative sum of the index over the duration of the event. The intensity of a drought or wetting event is its severity divided by its duration and is considered the average index or ‘rating’ of that event. To robustly investigate the significance of drought trends, a modified Mann-Kendall test was employed (Mann, 1945; Wilks, 2011) to avoid inflated p-values due to the underestimation of the test statistic variance (Hamed and Ramachandra Rao, 1998). Then, the Theil-Sen slope estimate was used to identify the magnitude of the trend (Theil, 1950). The two-sample Kolmogorov-Smirnov test was implemented to test the hypothesis that the distributions of a metric calculated from drought or wetting events during different time periods come from the same continuous distribution (Massey, 1951). Statistical significance was assessed at a level of 5% for these tests.

2.4. Empirical orthogonal function analysis

For this study, grid point location and SPEI values were the variables and observations, respectively, for the EOF analysis. The resulting orthogonal eigenvectors, also referred to as EOFs, point in the direction in which the data vectors exhibit the most variability. The principal components (PCs), which represent how EOFs evolve through time, are obtained by projecting the EOFs onto the original SPEI data. EOFs often exhibit characteristics that hamper their utility to isolate individual patterns of variation, such as domain shape or size dependence (Richman, 1986). Because weather in the Great Plains is generally dominated by large regional atmospheric processes, the orthogonality constraint on the eigenvectors can lead to problems with interpretation, especially for the second and subsequent PCs (Wilks, 2011). Because of the limitations of EOF analysis in the Great Plains, a retained number of EOF loadings (each retained EOF scaled by the square root of its eigenvalue) were rotated using Varimax rotation (Kaiser, 1958; Preisendorfer and Mobley, 1988). Varimax rotation redistributes the variance among rotated EOFs (rEOFs) and PCs (rPCs) and attempts to simplify the rEOFs by pushing loading coefficients toward 0 or ± 1 . The loadings used for this rotation result in nonorthogonal rEOFs and rPCs (Wilks, 2011) that are more regionally localized and highly correlated to the original SPEI data than the unrotated EOFs and PCs.

Several selection methods are available to determine the number of EOFs that capture most of the variability without significant loss of information. These methods can be divided into three classes: rules based on the size of the last retained eigenvalue (Hannachi et al., 2007), hypothesis-testing (Preisendorfer and Mobley, 1988), and the structure of the retained principal components (Wilks, 2011). One commonly used selection rule is North's Rule of Thumb (North et al., 1982) which uses the sampling error of each eigenvalue to determine non-degenerate EOFs. However, North's Rule of Thumb and other selection methods such as Kaiser's Rule or Rule N (Overland and Preisendorfer, 1982) use the size or sampling properties of the eigenvalues and do not adequately fit the objective of this study because they do not use properties of the EOFs after rotation. We argue that the primary utility of rEOFs in drought analysis is their ability to identify subregions of similar variability through time without the constraint of orthogonality and propose that a more useful criterion is the correlation of the rPCs with the original data. When subregions are identified with rPCs that are highly correlated to the original data, drought characteristics can be generalized across large land areas. As the number of EOFs rotated increases, the number of subregions identified increases, and correlation coefficients increase. At some rotation, there is no significant improvement in the correlation coefficients. Based on this observation, we propose a new rule to identify the rotation at which this occurs.

2.5. Selection rule for determining the number of rotated EOFs

The selection rule begins when a selected number of leading EOFs (N) are rotated (usually two). At each of the 891 grid points, the original standardized drought dataset is correlated with all N rPC time series, using the absolute value of the correlation coefficients. For each grid point, the rPC time series with the highest correlation is reported as i , which is designated as an integer between 1 and N . After all grid points have been matched with a single rPC, subregions can be identified by grouping together grid points with the same i , forming a subregion mask. Next, $N + 1$ leading EOFs are independently rotated, and the same procedure is applied when N were rotated. The subregion mask created using $N + 1$ leading rPCs is projected onto the grid of correlation coefficients that was calculated during the rotation of N EOFs. This projection creates two samples of paired correlation coefficients corresponding to the subregions in the current and previous rotation.

For each subregion j identified in the rotation of $N + 1$ EOFs, the difference between the current and previous correlation coefficients

from each rotation at each point in the subregion is calculated, and a sign test is performed to test the null hypothesis that the distribution of differences (D_j) has zero median against the alternative that the median is not equal to zero at a significance level of 1%. If the result of the sign test is statistically significant, H_j is recorded as,

$$H_j = \begin{cases} 1, & \text{median}(D_j) > 0 \\ -1, & \text{median}(D_j) < 0 \end{cases}$$

If the test is not significant, H_j is recorded as zero. When $\sum_{j=1}^{N+1} H_j > 0$ there was at least one subregion that had an improvement in the median correlation when an additional EOF was rotated. N is incremented by one, and the procedure is repeated until the first occurrence when the criteria $\sum_{j=1}^{N+1} H_j < 0$ is met, indicative that the inclusion of an additional rEOF weakened the overall relationship between subregion rPCs and the original SPEI data. The number of desirable rEOFs is given as N , and the procedure concludes. No statistically significant gains in information were made in the subregions identified using $N + 1$ rEOFs, and the subregions have become relatively stable. It is important to note that there are cases when $\sum_{j=1}^{N+1} H_j = 0$ at a rotation followed by $\sum_{j=1}^{N+1} H_j > 0$ when additional rEOFs are included, which is the rationale for using the criteria $\sum_{j=1}^{N+1} H_j < 0$. Also, if there were N rEOFs, there might be fewer subregions identified based on this correlation procedure.

After the final number of rEOFs to rotate has been decided, smooth boundaries between subregions can be drawn by interpolating the maximum correlations. Correlations should be presented with subregion boundaries to illustrate the strength of the relationship of these rPCs with the original SPEI data. In some heterogeneous cases, non-continuous subregions can be identified due to similarities in drought dynamics separated at distance, and these cases should be carefully examined when constructing a subregion mask.

The numerical magnitude and sign of the standardized rPC of each subregion can be interpreted as a drought index that possesses statistical properties similar to the input dataset (i.e., the SPEI data). Thus, the same seasonal and full-record drought characteristics that were calculated for the SPEI can also be calculated for the rPC, allowing for drought and wetting event detection and statistical analysis across spatial scales larger than a single grid point. Full-record rPCs were used to calculate drought and wetting event durations, severities, and intensities for events occurring in two periods (1901–1957 and 1958–2015) to assess changes in the distributions of drought metrics. To assess whether seasonal drought variability has remained stationary over time, an rEOF analysis was conducted using a fixed number of rEOFs on a 50-year moving window (starting 1901–1950, 1902–1951, and continuing until 1966–2015). If the total variance explained by the rEOFs for each individual analysis stays approximately the same, then climatic features that influence drought across the Great Plains have remained relatively stable through time.

3. Results

3.1. Climate trends and drought statistics

CRU winter and summer growing season maximum temperature significantly increased between 1901 and 2015 across a majority of the northern and western High Plains (Fig. 2a(i) and a(ii)). The strongest rates of warming (0.2 – 0.3 °C decade⁻¹) occurred across the foothills of the Rocky Mountains in New Mexico, Colorado, and Wyoming in the summer (Fig. 2a(ii)). Spatial distribution of trends during the summer and winter growing seasons were relatively similar, but across North Dakota and Minnesota, trends were larger during the winter than during the summer. During the summer season, there were also several notable areas in the eastern Great Plains that experienced significant decreases in maximum temperature. Minimum temperature during the winter increased at a faster rate than during the summer (Fig. 2b(i) and

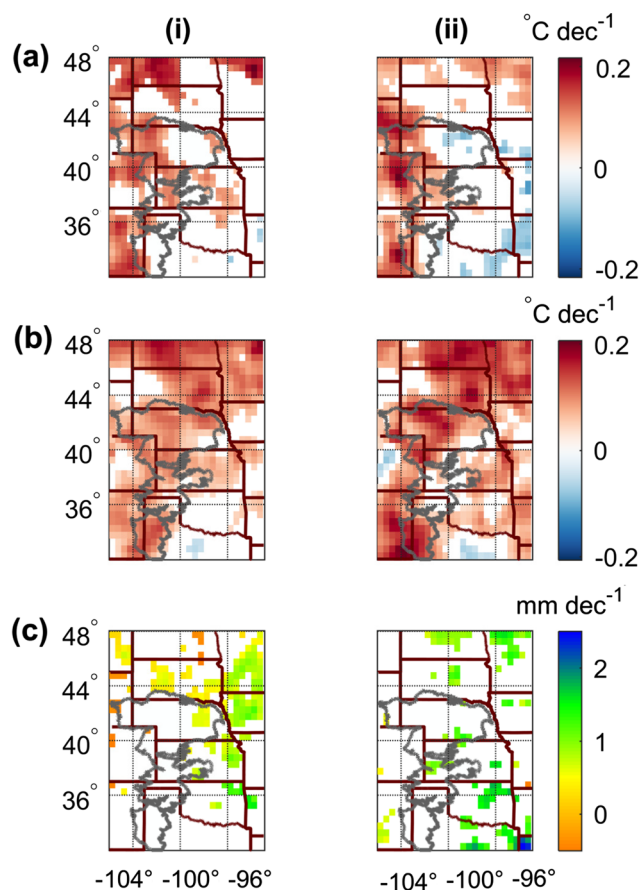


Fig. 2. Growing season trends for (a) maximum temperature, (b) minimum temperature, and (c) precipitation between 1901 and 2015 for (i) Nov. – Apr. (winter) and (ii) May – Oct. (summer). Only grids with statistically significant trends using the modified Mann-Kendall test ($\alpha = 0.05$) are shaded. Grids with non-significant trends are unshaded (i.e., white).

b(ii)), and the proportion of grid points showing a statistically significant increasing trend was greater for minimum temperature than for maximum temperature (Fig. 2a and b). The largest differences between winter and summer minimum temperature trends occurred in eastern South Dakota, North Dakota, Minnesota, and New Mexico. There was also more significant warming in the southeast Plains over Arkansas during the summer than the winter. These warming trends during the summer in the southeast are in direct contrast to the cooling trends displayed by maximum temperatures.

Spatial distributions of growing season precipitation trends for both seasons were more variable and isolated (Fig. 2c(i) and c(ii)). Of the grids with a statistically significant trend in precipitation, most exhibited a positive trend (Fig. 2c(i) and c(ii)). Isolated areas east of the -100° meridian during the summer increased at the highest rates, and the rate of increase exceeded 2 mm decade^{-1} across northwest Louisiana (Fig. 2c(ii)). During the winter growing season, a small number of grids west of the -100° meridian had a modest decrease in precipitation (-0.2 to $-0.5 \text{ mm decade}^{-1}$ in Fig. 2c(i)).

When evaluated using a threshold of -0.5 , the 3-month SPEI data revealed that there were on average 143 droughts per grid point (approximately 1.2 times per year in the Great Plains) with a standard deviation of 8.8 in the Great Plains between 1901 and 2015. When the period was divided into three time intervals of equal duration excluding 1901 (1902–1939, 1940–1977, and 1978–2015), the average number of drought events per grid point was approximately 48, 49, and 41, respectively. Notably the last 38 years had significantly fewer drought events than the previous two periods, which was offset by an increase in the number of wet events using a threshold of 0.5 (53 wet events for

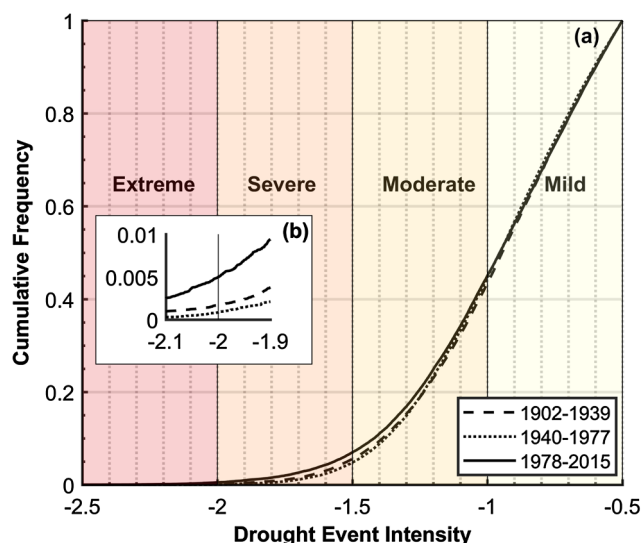


Fig. 3. (a) Empirical cumulative frequency distributions for Standardized Precipitation-Evapotranspiration Index drought event intensities across the entire study area for three periods: 1902–1939, 1940–1977, and 1978–2015. Drought events were grouped based on the month each drought event terminated. (b) Cumulative frequency distribution magnified near the extreme drought boundary.

1978–2015 vs. 48 for 1902–1939). Empirical cumulative frequency distributions (ECFD) of SPEI drought event intensities for these three time intervals are shown in Fig. 3a. The two-sample Kolmogorov-Smirnov test was statistically significant for all pairwise comparisons (p -values $< 10^{-5}$). These distributions demonstrate that of the drought events that occurred between 1978 and 2015, moderate, severe, and extreme drought events occurred at a higher frequency than in previous periods. While the number of drought events decreased in recent years, the intensity of those events increased. Divergence between time interval ECFDs is evident beginning at intensities of around -1.75 , reaching maximum separation around the transition between severe and moderate drought categories.

All three time intervals had less than 10% of all droughts rated severe or extreme, and 35–40% of all drought events were rated as moderate. Notice that 0.18%, 0.09%, and 0.50% of all drought events are categorized as extreme for the periods 1902–1939, 1940–1977, and 1978–2015, respectively (Fig. 3b). In context of the study area and the number of events per period, roughly 21% of grids experienced a drought event that rated on average as extreme between 1978 and 2015 while only 4% did between 1902 and 1939. Combining the information contained across all grid points shows the overall status of the Great Plains; however, more relevant information can be acquired by analyzing the drought and wetting dynamics contained in subregions that contain distinctive information about drought variability.

3.2. Seasonal rEOFs

3.2.1. Spring and summer

Thirteen EOFs were selected for rotation using spring SPEI, resulting in 10 subregions of similar drought variability that explain about 85% of the total drought variability (Fig. 4a). Correlation coefficients of rPCs with the original SPEI data for grid points within subregions were generally greater than 0.75. These subregions span administrative units and political boundaries. For example, subregion 1, which covers most of central and western Kansas, also includes an extension of land in interior southern Colorado (east of subregion 7 in Colorado and northern New Mexico). It should be noted that the overall correlation in this area of Colorado comparatively lower, and it may be the result of high variability or it possessing characteristics more in common with

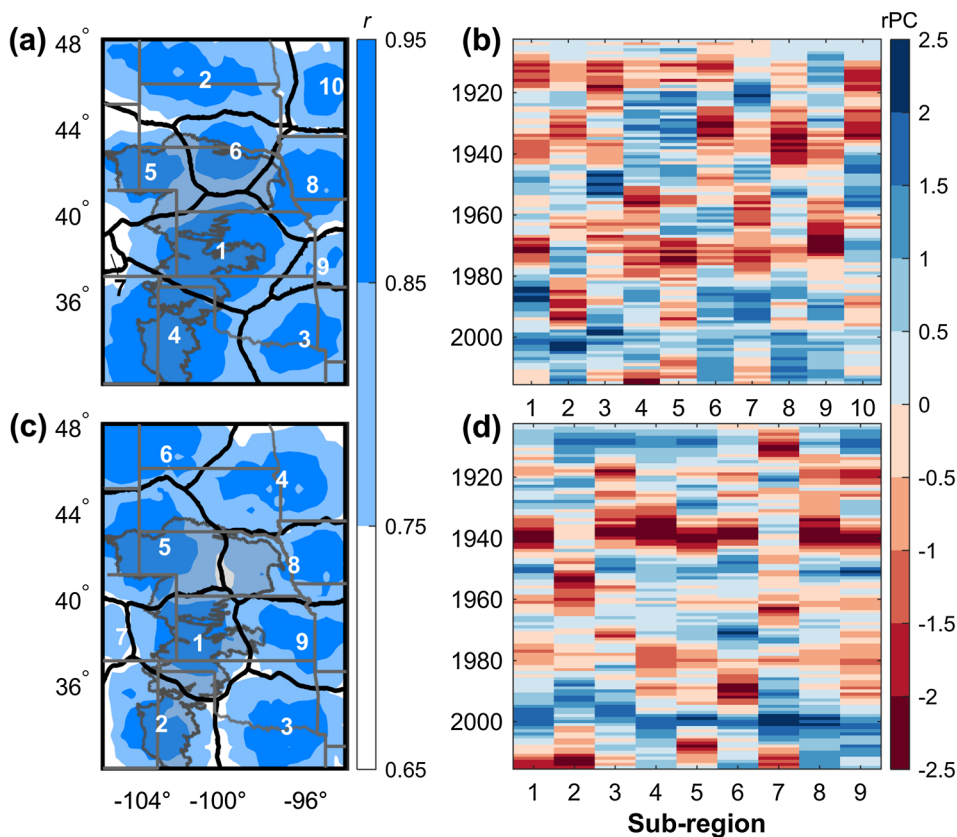


Fig. 4. Subregions identified in the U.S. Great Plains for (a) spring and (c) summer drought variability and the standardized rotated principal component (rPC) time series for subregions in (b) spring and (d) summer. Each subregion in (a) and (c) has a number that corresponds to its rPC time series in (b) and (d), respectively. Subregion and state boundaries are black and gray, respectively, and the Ogallala Aquifer is shaded gray. The left color bar represents the correlation coefficients for each subregion's rPC time series on the right and the original drought dataset at individual grid points. The right color bar represents the magnitude and sign of each rPC time series from 1901 to 2015. Negative and positive rPC values indicate dry and wet conditions, respectively. Time series of rPC are 10-year running average filtered (used as a smoother to remove interannual variability and retain decadal variations). (For interpretation of the references to color in this figure legend, the reader is referred to the web version of this article.)

areas west of the study domain. The area along subregional boundaries in western South Dakota demonstrate low correlation ($r < 0.75$), illustrating that the variability exhibited in these areas is not explained as well as other areas in the domain using this procedure.

The spring rPC time series demonstrate clear differences between subregion seasonal drought and wet spell onsets, durations, and severities (Fig. 4b). The time series also highlight periods when subregions experienced similar drought conditions (e.g., drought between 1960 and 1980). Based on severity and duration, subregion 9 centered on eastern Kansas and Missouri experienced the longest period of sustained extreme spring drought during the 1960s. Spring droughts occurring during the 1960s and 1970s appear to have had somewhat larger areal coverage as evident by the red bands across most subregions in Fig. 4b. The 2011–2012 springtime drought was the worst ($rPC < -2$) for subregion 4 in the Texas Panhandle. Overall, each time series shows its own unique drought characteristics with differences in onset, duration, and intensity of spring drought events.

Fourteen EOFs were selected for rotation using summer SPEI data, resulting in 9 subregions of similar drought variability that explain about 82% of the total drought variability (Fig. 4c). All subregions have at least one grid point with a correlation coefficient of 0.75 or greater, and the area in central Colorado (subregion 7) demonstrates a much stronger relationship with its rPC than subregion 7 in spring (Fig. 4a). The orientation of subregions is notably different in the summer than during the spring (Fig. 4a and c). There is a nearly vertical axis at about the -100° meridian that extends from the southern portion of the study domain into central Nebraska.

For most of the Great Plains, summer drought in the 1930s (Fig. 4d) was notably extreme and had much higher regional coverage than spring drought. The Dust Bowl era of the 1930s contained some of the driest and hottest growing seasons in modern U.S. history, which would have had significant negative impacts on crop production (Glotter and Elliott, 2016). Subregions across Kansas and northward showed the most extreme decadal drought conditions during this time. Summer

drought conditions between 2005 and 2015 were notably drier for subregions 1, 2, 5, and 7 extending across the High Plains.

3.2.2. Fall and winter

Fifteen EOFs were selected for rotation using fall SPEI data, resulting in 12 subregions of similar drought variability that explain about 85% of the total original drought variability (Fig. 5a). The orientation of subregions resembles the orientation for spring rEOFs (Fig. 4a) with boundaries angled towards the northeast. There are correlation coefficients greater than 0.75 within all subregions except subregion 9, which is located along the Minnesota and Iowa border. This area exhibits lower correlation during fall than spring or summer. Other areas exhibiting low correlation were in south central Nebraska and north central Kansas. The rPCs for each subregion demonstrate that the multi-decadal period starting in 1940 and ending during the early 1960s was notably dry (Fig. 5b), while 1970s fall conditions were overall wet with the most notable drought occurring in subregions 1 and 8 in the mid-1980s.

Eighteen EOFs were selected for rotation using winter SPEI data, resulting in 10 subregions of similar drought variability that explain about 88% of the total original drought variability (Fig. 5c). The subregions constructed in the southern plains are quite large compared to those for spring, summer, and fall. Notably there is one that spans across most of the portion of Texas within the study domain (subregion 1). This is significant because for the other seasons, the area of the domain that includes Texas is divided across the low rolling plains. Additionally, subregion 4 dominates most of Kansas, southeast Nebraska, and Iowa. These large subregions also demonstrate strong correlation, highlighting the broad and homogenous influence of synoptic features during the winter in the southern plains. Drought planners may be able to consolidate resources when assessing winter mitigation strategies. The area that demonstrates the most variability lies across Colorado and Minnesota. Upon examination of the rPC time series, the period between 1960 and 1980 was notably the driest for most

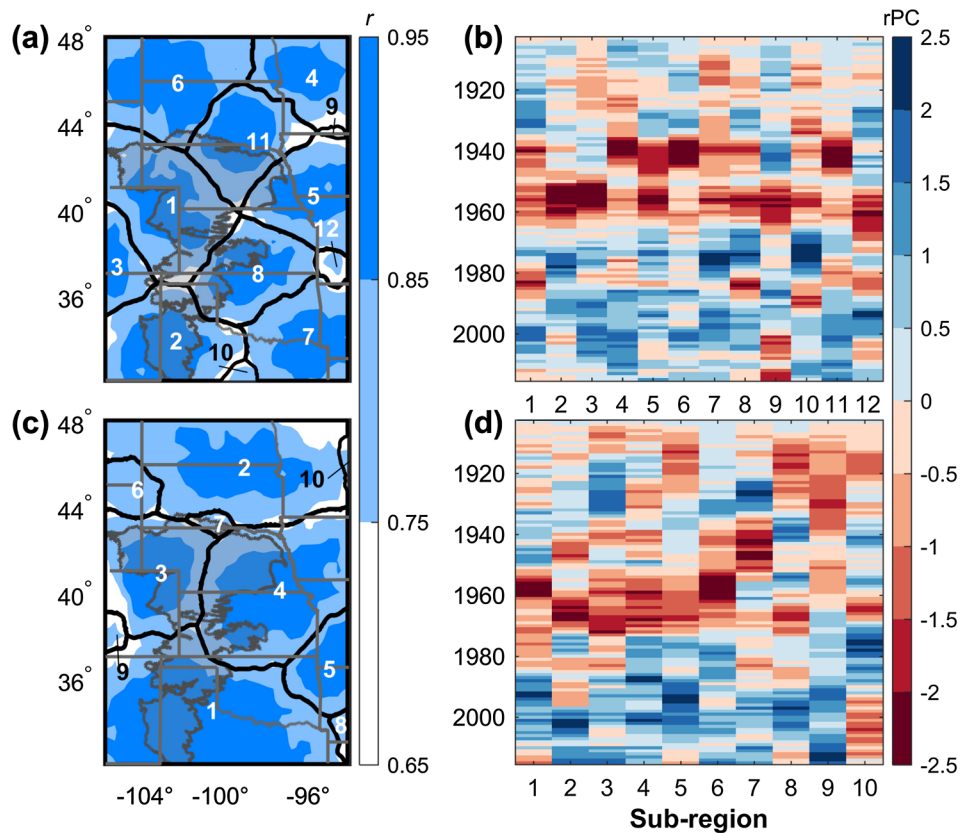


Fig. 5. Same as Fig. 4 but for (top) fall and (bottom) winter.

subregions (Fig. 5d). Subregion 6 across western South Dakota in the northern Great Plains experienced the longest duration of extreme decadal drought of any region during the late-1950s and early-1960s, followed closely by subregion 1 during the mid to late-1950s.

3.2.3. Seasonal trends

For springtime drought conditions, subregion 6 in north central Nebraska had a statistically significant trend of 0.06 rPC decade⁻¹ (Fig. 6a). During the summer, subregion 8 across eastern Nebraska and Iowa had a statistically significant trend of 0.09 rPC decade⁻¹ (Fig. 6b). Trends during the fall and winter showed the strongest statistical evidence among all seasons (Fig. 6c and d). Subregions 3 (centered on southern Colorado), 4 (centered on Minnesota), 7 (centered on eastern Texas), and 11 (centered on southeast South Dakota) demonstrated significant wetting trends of 0.06, 0.06, 0.08, and 0.09 rPC decade⁻¹ during the fall, respectively (Fig. 6c). Winter subregions 5, 6, and 9 also demonstrated statistically significant wetting trends of 0.07, 0.06, and 0.16 rPC decade⁻¹, respectively, and all three are separated at distance across the domain and demonstrate no clear spatial pattern (Fig. 6d). As a whole, seasonal trend analysis showed that either some regions in the Great Plains have trended towards wetter conditions since 1901, or they do not have significant trend values. However, it is interesting to note that some areas across the Great Plains were characterized by temporal trends that were positive and negative in different seasons. For example, areas in northwest Nebraska demonstrated wetting and drying in winter (subregion 6) and spring (subregion 5), respectively. These results emphasize the importance of seasonal analysis which has major implications for the agricultural community who depend on timely rainfall during different growing seasons.

3.3. Full-record rEOFs

Fourteen EOFs were selected for rotation when using the full-record

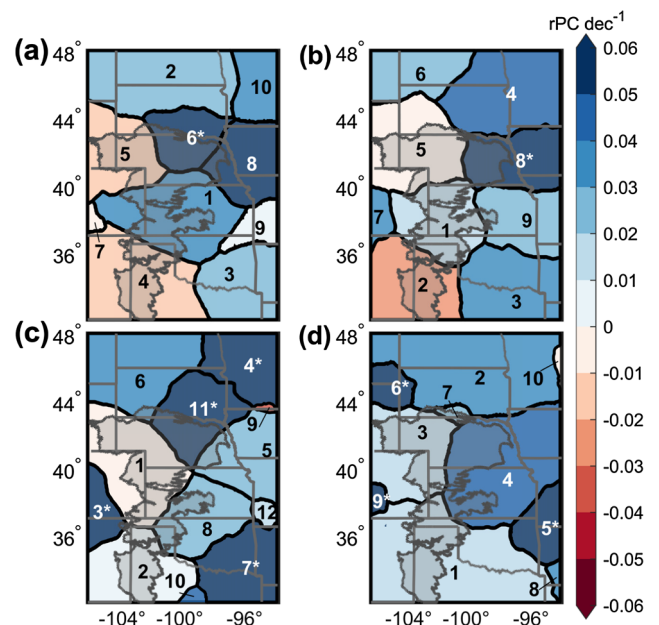


Fig. 6. Theil-Sen slope estimates for the rPCs associated with the subregions in Figs. 4 and 5 for (a) spring, (b) summer, (c) fall, and (d) winter. Subregions with a * indicate statistical significance ($\alpha = 0.05$) determined using the modified Mann-Kendall test.

SPEI data resulting in 10 subregions of similar drought variability that explain about 87% of the total drought variability (Fig. 7a). All rPCs (excluding 9) for each subregion are highly correlated to the original SPEI data ($r > 0.85$). Spatially, the correlation matrix illustrated that the rPCs for most subregions in the Great Plains were significantly correlated ($0.05 < r \leq 0.7$) (Fig. 7b). The two pairs of subregions that

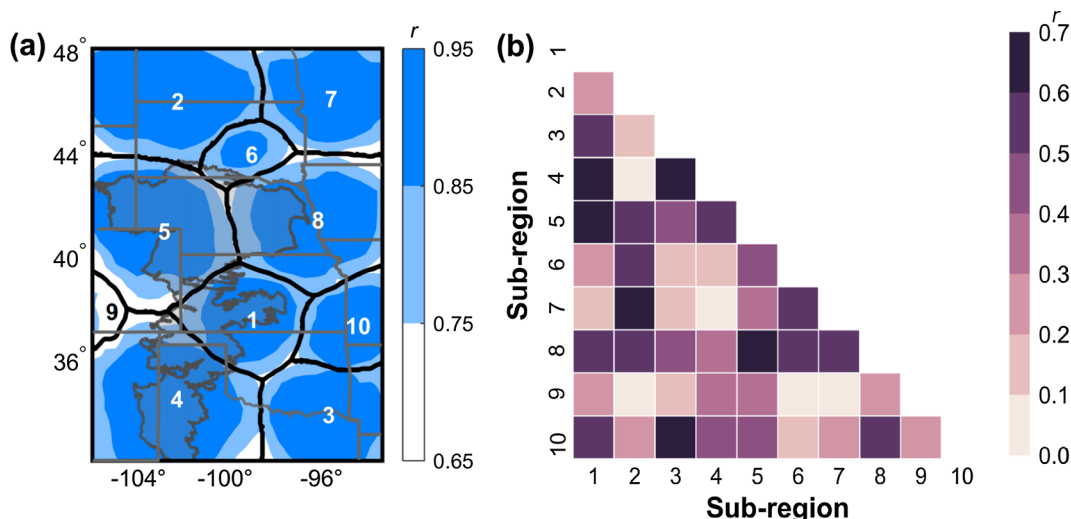


Fig. 7. (a) Subregions identified for full-record Standardized Precipitation-Evapotranspiration Index (SPEI) and (b) the correlation coefficients between subregion rPC time series.

have the strongest relationship are 2 and 7 and 5 and 8 ($0.6 < r \leq 0.7$). In contrast, subregions 4 and 7 across the southern Ogallala Aquifer and Minnesota, respectively, have non-significant correlations. The SPEI drought conditions of subregions 4 and 7 act independently. This demonstrates that summarizing the short-term drought variability of the Great Plains as a single region would be a mischaracterization of the complexities that exist in this region, particularly across the southern High Plains and northern Great Plains.

For each subregion’s full-record rPC, distributions of drought events and corresponding metrics were calculated using thresholds of -0.5 , -1.0 , -1.5 , and -2.0 for the periods before and after 1958. Likewise, distributions of wet events were calculated using thresholds of 0.5 , 1.0 , 1.5 , and 2.0 . The distributions for the thresholds of -0.5 and 0.5 and results of the two-sample Kolmogorov-Smirnov test are presented in Fig. 8. There is no statistical evidence for changes in drought metric distributions between these two periods at this threshold (Fig. 8a). In contrast, there is evidence of a distribution shift towards more severe

(p-value: 0.04) and intense (p-value: 0.01) wet events between 1958 and 2015 across Minnesota in subregion 7 (Fig. 8b).

At thresholds less than -0.5 and greater than 0.5 (results not shown), only a few subregions had statistically significant changes in distributions for drought event metrics. Differences in drought event intensities between the two periods for subregion 2 at a threshold of -1.0 were statistically significant (p-value: 0.02). This is an indication that the intensity of moderate drought events increased during 1958–2015 across western North Dakota, South Dakota, and eastern Montana. At a threshold of -1.5 , the intensities of drought events in subregion 8 were statistically significant, indicating an increase in drought event intensity during 1958–2015 (p-value: 0.04).

3.4. Temporal changes in drought variability

To examine temporal changes in drought variability, ten leading REOFs were retained for this analysis based on the number of subregions

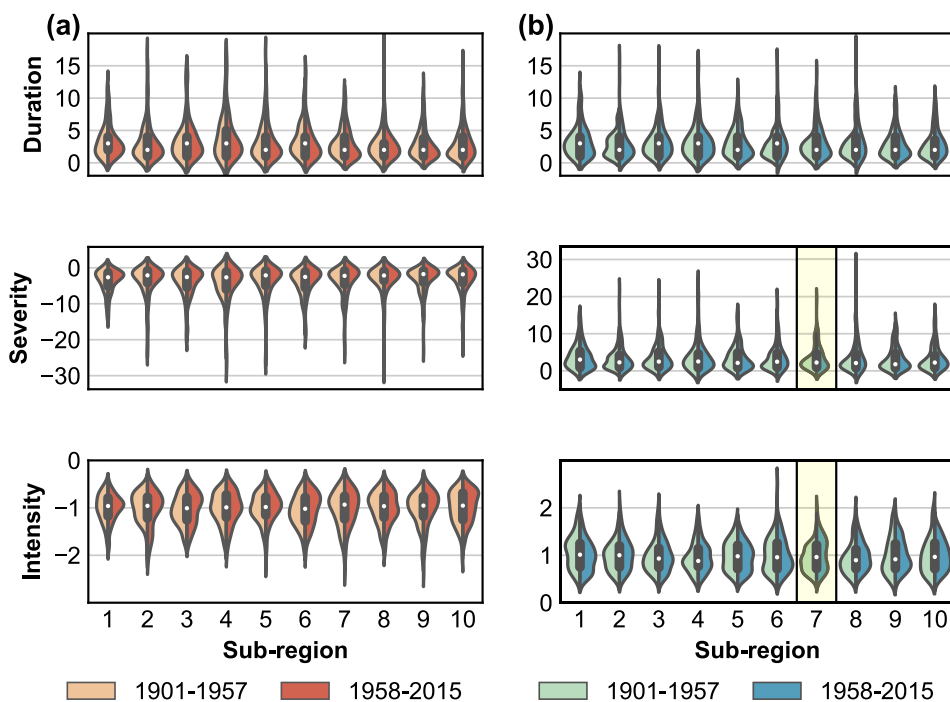


Fig. 8. Violin plots of (a) drought and (b) wet event durations (months), severities, and intensities for subregions shown in Fig. 7 using thresholds of (a) -0.5 and (b) 0.5 . For each subregion, the distributions for each drought event metric are split into the periods 1901–1957 and 1958–2015. The white circle for each violin is the joint median for both periods. Distributions that significantly changed ($\alpha = 0.05$) between periods are highlighted in yellow. (For interpretation of the references to color in this figure legend, the reader is referred to the web version of this article.)

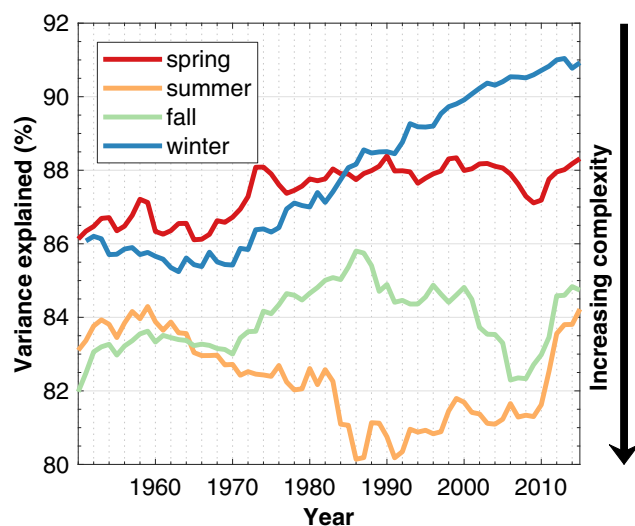


Fig. 9. The seasonal variances explained by 10 EOFs using a 50-year moving window for the U.S. Great Plains from 1901 to 2015. The x-axis labels (year) indicate the end year of each moving window in the EOF analysis (e.g., 1960 corresponds to 1911–1960). Lower variance explained corresponds to a higher complexity in the spatial-temporal drought features during that period, whereas higher variance corresponds to lower complexity.

identified previously, and a 50-year moving window starting from 1901 was used to calculate the total variance explained for each window. A decrease in the amount of variance explained by the same number of rEOFs is an indication that the space-time variability of drought increased because more rEOFs must be retained to explain the same proportion of variability. Fig. 9 shows how the total variance explained by 10 rEOFs has changed over time by season. The variance explained by summer rEOFs changed significantly between the periods 1932–1981 and 1937–1986, decreasing from 82% to almost 80% within a period of several years. However, it steadily rebounded between 1941–1990 and 1966–2015. The variance explained by fall rEOFs steadily increased and decreased over the period, demonstrating little overall differences. One explanation for the increasing variability is the change in coverage of major drought and wetting events. Results from the seasonal rEOF time series showed that persistent and widespread droughts (e.g., in the 1930s and mid-to-late 1950s) affecting most subregions occurred less frequently in the latter half of the twentieth century. Subregions experienced more localized drought and wetting events of variable duration, severity, and intensity, increasing the space-time variability in EOF analysis. The sharp rebound starting around 1961–2010 during the summer was most likely due to the major drought event between 2011 and 2012, which had substantial coverage across most of the Great Plains. If historical trends continue, and seasonal drought becomes more variable, a more diverse set of resources and strategies may be required to deal with its impacts.

Overall, winter and spring showed an increase in variance explained by the rEOFs while the summer drought has become more complicated (i.e. more difficult to explain) in terms of variability (Fig. 9). Temporal variations of drought variability explained for the winter season were relatively smaller than those in other seasons, indicating that the effects of climatic structures that drive drought variability changed less rapidly year-to-year in winter. Thus, this suggests that spatially, the effects of drought and wetting events became more homogenous. Should this homogeneity continue among winter events across the Great Plains, there is the potential for resource managers to consolidate resources to mitigate impacts. However, when drought or wetting events do occur, their impacts could be more widespread.

4. Discussion

Our results showed that temperatures have significantly increased for a large portion of the Great Plains during the summer and winter growing seasons while trends in precipitation have significantly changed for only isolated areas of the Great Plains (Fig. 2). The seasonal rPC trends from EOF analysis demonstrated that only some subregions experienced statistically significant changes in drought conditions, and the rPC trends more closely resembled the patterns displayed by the precipitation trends than the temperature trends. While much of the western Great Plains demonstrated statistically significant trends in temperature (Fig. 2a and b), only a few grid points had statistically significant precipitation trends (Fig. 2c). In the EOF analysis, the rPC trends of seasonal subregions in the western Great Plains were also not significant. Many areas in the eastern Great Plains that demonstrated positive trends in precipitation (Fig. 2c) also demonstrated significant wetting in the EOF analysis (Fig. 6). It is apparent that the warming that occurred in the western Great Plains did not significantly change the monthly differences between precipitation and PE that are inputted into the SPEI calculation, emphasizing that precipitation is most likely the dominant driver of SPEI variability in the Great Plains, which is similar to the results from previous work (Livneh and Hoerling, 2016). Trend analysis also highlighted that some subregions covering similar areas demonstrated both drying and wetting trends depending on the season analyzed. Based on these results, we contend that analysis of the seasonal rPC trends instead of the full-record rPC trends has more practical implications for agriculture because full-record analysis can mask seasonal trends that are diametrically opposed, which would be misleading for crop producers. While previous drought EOF studies have focused more on the full drought record than the seasonal drought record, we argue that drought analysis should, where possible, be conducted seasonally to truly understand the complexity of drought dynamics.

An important caveat to acknowledge is that the trends calculated in this study may have been slightly different if another gridded dataset product was chosen for analysis. Because gridded datasets process station observations differently, it is important to consider the uncertainties in trends that result from the methodology used in dataset construction (Wang et al., 2017). For example, CRU TS datasets are constructed using the Climate Anomaly Method (Peterson et al., 1998), which requires station data to meet a minimum number of observations for observed climatology. At each time step, available observation anomalies are gridded to $0.5^\circ \times 0.5^\circ$ resolution using triangulated linear interpolation, which are converted to absolute values using the 1961–1990 climatology (Harris et al., 2014). Analysis of temperature trends over the period 1901–2015 (not shown) demonstrated relatively good spatial agreement among other higher resolution datasets such as the Parameter–Elevation Regressions on Independent Slopes Model (PRISM) (Di Luzio et al., 2008) and VOSE (Vose et al., 2014). Notably maximum temperature trends calculated from PRISM exhibited a higher coverage of grid points with significant decreases in temperature in the eastern areas of the Great Plains. PRISM does not adjust for changes in instrumentation (Wang et al., 2017), which may explain discrepancies among products. Precipitation trends among CRU, PRISM, VOSE, and Global Precipitation Climatology Centre (GPCP) exhibited much stronger agreement than minimum and maximum temperature.

There have been several proposed explanations for the observed wetting trends in the Great Plains and Midwest. Some studies suggest that widespread expansion of irrigation and cropland that occurred during the 1950s enhanced summer precipitation by increasing atmospheric moisture and moisture convergence (Alter et al., 2015; Alter et al., 2017). Other research suggests that the variability of the Great Plains low-level may have played a role in the alteration of precipitation patterns (Wang and Chen, 2009). Rising temperatures resulting from an increase in global greenhouse concentrations have also been linked to an increase in atmospheric water vapor across areas of the

Great Plains, leading to an increase in the frequency of heavier rainfall events (Groisman et al., 2004; Villarini et al., 2012). While our study cannot directly explain the trends we observed, our results fit well within the current literature for this region. Although not explored in great detail, dividing the entire period of record into smaller moving windows, performing the EOF analysis, and examining changes in subregion patterns through time may provide insight into changes in synoptic structures that have dominated the Great Plains since instrumental records began.

Seasonal EOF analysis also demonstrated differences in the spatial patterns of the subregions. This is additional evidence for conducting seasonal EOF analysis because it provides insight into the different processes that dominate seasonal drought variability in the Great Plains. These processes were more apparent during the rotation of selected EOFs. Rotation of two leading EOFs demonstrated that the dominant seasonal subregions of drought variability in the Great Plains occur in the northern and southern plains. This division may be physically explained by the relative influence of sea surface temperatures in the Pacific Ocean for these two regions. Previous studies have found that drought variability in the southern Great Plains is more sensitive to changes in equatorial Pacific sea surface temperatures than drought variability exhibited in the northern Great Plains, which may respond greater to internal atmospheric variability (Hoerling et al., 2009). Warming and cooling of the sea surface temperatures in the Pacific Ocean can generate changes in the prevailing circulation patterns that transport moisture from this source region (Borchert, 1950). Rotation of three EOFs divided the previously identified subregions into areas that resemble the synoptic structures that dominate weather. For example, during the summer in the southern plains, subregions are sharply divided at the -100° meridian, representing the western boundary of the northward transport of gulf moisture by the low-level jet in the eastern Great Plains. For the winter season, subregions have boundaries that resemble synoptic fronts, which result from the cyclonic movement of air masses across the Great Plains. These physical modes of variability exhibited by the differences in seasonal synoptic structures provide a physical explanation of the subregion patterns in the EOF analysis.

Based on the total amount of drought variability in the Great Plains, the selection rule proposed in this study identified 9–12 subregions. Compared to the Karl and Koscielny (1982) study, the number of subregions identified in our analysis for the Great Plains was equal to or larger than the nine identified for the entire United States. However, the authors in that study chose the number of EOFs to retain for rotation based on the original resolution of the dataset, which included only 60 grid points across the entire U.S. In addition, none of the subregions had rPCs that were strongly correlated with drought data in the central Great Plains. Other studies in areas outside the U.S. used North's Rule to identify the number of EOFs to retain for rotation and then constructed subregions using cluster analysis or examination of the coefficients of the rEOFs (Cai et al., 2015; Raziei et al., 2010). We identified six to seven seasonal subregions using North's Rule in the Great Plains, which was less than the number identified using our selection rule. However, the correlation coefficients across subregions using North's Rule were lower, particularly in the areas identified in our analysis along subregion boundaries. Our rule could identify subregions across these areas that significantly improved correlation with the original data across most of the Great Plains. Analysis of the statistical properties of the rPCs in this study also demonstrated that the subregions had unique characteristics, such as different drought or wetting trends, providing strong evidence for their inclusion in drought monitoring. Because the selection rule proposed in this study tests the differences in correlation coefficients within subregions in sequential rotations, we argue that they represent the best subregions of drought variability that can be obtained by EOF analysis. This was exhibited by the high correlation of the rPCs with the original SPEI data. Areas that consistently had lower correlations such as Colorado indicate that dimensional reduction of drought variability in this region was difficult to achieve, which may be

expected given that this area represents a high degree of precipitation variability that results from the orographic lift of the Rocky Mountains that may not be represented adequately at the resolution of the CRU dataset. Because drought indices are usually standardized, the rPCs can be interpreted as a meaningful drought index, which has numerous advantages when the goal is to proceed beyond subregion identification. Highly correlated drought rPCs for identified subregions can be examined for detection of climate change signals, which has implications for drought management due to the information gain over a large area.

The design and properties of the selection rule in this study make the rule adaptable to different applications of drought monitoring or other dimension reductions of space-time geophysical data. We recognize that statistical tests other than the sign test could be utilized to determine improvements in the subregion correlation coefficients. Other tests that examine characteristics of a distribution other than the median might provide further insight into identifiable subregions, although the characteristics of those distributions would need to be examined to ensure that test assumptions are reasonably satisfied. Manual adjustments may also be desired if any subregions identified do not add useful information. Without implementation of the sign test, the upper-limit of the number of identified subregions using all 891 EOFs for rotation was approximately 18–20. The small, additional subregions extended across areas with low correlation in the seasonal analysis. However, the correlation coefficients between those rPCs and the original SPEI data were still smaller than the coefficients for the main subregions and explains why they were excluded in this analysis using our selection rule. The selection rule is also relatively robust to changes in the size of the domain. Increasing the domain size can change regional features along the domain boundary, and reconstructing the regional patterns produced using the smaller domain generally requires a larger number of rEOFs because additional variability is introduced. These properties make it suitable for applications in other areas of the world at larger and smaller spatial scales to identify subregions of variability of a geophysical variable through time. Because of the properties demonstrated by this selection rule and its ability to identify subregions that have physical basis in the synoptic structures that drive drought variability, we argue that future drought management strategies and planning would be more advantageous in terms of these subregions.

5. Summary and conclusions

There has been an increase in growing season maximum and minimum temperatures across many areas of the Great Plains between 1901 and 2015. The greatest increases in growing season precipitation have been isolated to areas primarily east of the -100° meridian. Three-month SPEI drought event intensities increased in magnitude during the period 1978–2015 across the Great Plains although the number of events was lower compared to previous periods. Higher intensity droughts, while less frequent, will have negative impacts on agriculture as short-term and large water deficits occur in critical stages of crop growth. In contrast, the number of total wet events has risen in recent years, indicating an increased risk of excess moisture that may have major impacts on agriculture in the future.

Rotated EOF analysis using our selection rule identifies the main subregions of variability in the Great Plains and can be used to integrate drought monitoring information and inform drought management decisions at a local scale, especially when there are not sufficient in-situ climate stations. Our method produces subregions that are consistent with synoptic features and can be easily interpreted by drought management agencies. It has been shown that the number and spatial extent of subregions changes by season, reflecting the meteorological processes that dominate drought variability. Seasonal trends showed significant wetting for several subregions, and there is statistical evidence that the distributions of drought and wetting events for a few

subregions have changed between 1901–1957 and 1958–2015.

Changes in weather patterns both naturally and from the diverse set of human forcings (Council, 2005; Pielke et al., 2007) have the potential to alter the dominant features that affect drought variability in the Great Plains. The water resource community is considering the need to include changes in weather patterns from what occurred in the past to inform future management practices (Hossain et al., 2015). Analysis showed that drought variability was not stationary over the historical period. There is evidence of increased space-time drought variability since 1980 or later during the summer and decreased variability during the winter. Decision makers should interpret these changes in variability as an increase or decrease in the spatial drought complexities. If drought and wetting events become more variable across space and time, greater interregional cooperation will be desirable to accommodate for the wide-range of potential impacts. Decision makers in the Great Plains that have an understanding of these trends in variability will be able to adjust long-term resource management strategies that may help mitigate the economic and agricultural impacts throughout the twenty-first century.

Acknowledgements

This work was supported by the Kansas Water Resources Institute and the National Institute of Food and Agriculture, U.S. Department of Agriculture, under award number 2016-68007-25066, “Sustaining agriculture through adaptive management to preserve the Ogallala aquifer under a changing climate.” This manuscript is contribution number 18-239-J from the Kansas Agricultural Experiment Station. R. Pielke Sr. wants to thank CIRES and ATOC at the University of Colorado for providing him the venue to perform research. Dallas Staley is thanked for her standard outstanding job in editing.

References

- Alter, R.E., Fan, Y., Lintner, B.R., Weaver, C.P., 2015. Observational evidence that Great Plains irrigation has enhanced summer precipitation intensity and totals in the midwestern United States. *J. Hydrometeorol.* 16, 1717–1735. <https://doi.org/10.1175/JHM-D-14-0115.1>.
- Alter, R.E., Douglas, H.C., Winter, J.M., Eltahir, E.A.B., 2017. Twentieth century regional climate change during the summer in the central United States attributed to agricultural intensification. *Geophys. Res. Lett.* 45, 1586–1594. <https://doi.org/10.1002/2017GL075604>.
- Bjornsson, H., Venegas, S.A., 1997. *A Manual for EOF and SVD Analyses of Climatic Data*. Report No 97-1. McGill University, pp. 52.
- Bojariu, R., Velea, L.F., Cica, R.D., Dobrinescu, A.E., Birsan, M., Dumitrescu, A., 2012. Mechanisms of drought persistence in Romania in the climate change perspective. *Ann. Univ. Craiova-Biol., Horticult., Food Produce Process., Technol. Environ. Eng.* 17 (XVII).
- Bonaccorso, B., Bordini, I., Cancelliere, A., Rossi, G., Sutera, A., 2003. Spatial variability of drought: an analysis of the SPI in Sicily. *Water Resour. Manage.* 17, 273–296. <https://doi.org/10.1023/a:1024716530289>.
- Borchert, J.R., 1950. The climate of the central North American grassland. *Ann. Assoc. Am. Geogr.* 40, 1–39. <https://doi.org/10.2307/2561016>.
- Cai, W., Zhang, Y., Chen, Q., Yao, Y., 2015. Spatial patterns and temporal variability of drought in Beijing-Tianjin-Hebei metropolitan areas in China. *Adv. Meteorol.* 2015, 1–14. <https://doi.org/10.1155/2015/289471>.
- Cheval, S., Busuioc, A., Dumitrescu, A., Birsan, M.V., 2014. Spatiotemporal variability of meteorological drought in Romania using the standardized precipitation index (SPI). *Clim. Res.* 60, 235–248. <https://doi.org/10.3354/cr01245>.
- Colaizzi, P.D., Gowda, P.H., Marek, T.H., Porter, D.O., 2009. Irrigation in the Texas High Plains: a brief history and potential reductions in demand. *Irrig. Drain.* 58, 257–274. <https://doi.org/10.1002/ird.418>.
- Council, N.R., 2005. Radiative forcing of climate change: expanding the concept and addressing uncertainties. *The National Academies Press*, pp. 222.
- Dai, A., 2011. Characteristics and trends in various forms of the Palmer Drought Severity Index during 1900–2008. *J. Geophys. Res.* 116. <https://doi.org/10.1029/2010jd015541>.
- Di Luzio, M., Johnson, G.L., Daly, C., Eischeid, J.K., Arnold, J.G., 2008. Constructing retrospective gridded daily precipitation and temperature datasets for the conterminous United States. *J. Appl. Meteorol. Climatol.* 47, 475–497. <https://doi.org/10.1175/2007JAMC1356.1>.
- Easterling, W.E., Crosson, P.R., Rosenberg, N.J., McKenney, M.S., Katz, L.A., Lemon, K.M., 1993. Paper 2. agricultural impacts of and responses to climate change in the Missouri-Iowa-Nebraska-Kansas (MINK) region. *Clim. Change* 24, 23–61. <https://doi.org/10.1007/bf01091476>.
- Glatter, M., Elliott, J., 2016. Simulating US agriculture in a modern Dust Bowl drought. *Nat. Plants* 3, 16193. <https://doi.org/10.1038/nplants.2016.193>.
- Groisman, P.Y., Knight, R.W., Karl, T.R., Easterling, D.R., Sun, B., Lawrimore, J.H., 2004. Contemporary changes of the hydrological cycle over the contiguous United States: trends derived from in situ observations. *J. Hydrometeorol.* 5, 64–85. [https://doi.org/10.1175/1525-7541\(2004\)005<0064:CCOTHC>2.0.CO;2](https://doi.org/10.1175/1525-7541(2004)005<0064:CCOTHC>2.0.CO;2).
- Guttman, N.B., 1998. Comparing the Palmer drought index and the standardized precipitation index. *J. Am. Water Resour. Assoc.* 34, 113–121. <https://doi.org/10.1111/j.1752-1688.1998.tb05964.x>.
- Hamed, K.H., Ramachandra Rao, A., 1998. A modified Mann-Kendall trend test for autocorrelated data. *J. Hydrol.* 204, 182–196. [https://doi.org/10.1016/S0022-1694\(97\)00125-X](https://doi.org/10.1016/S0022-1694(97)00125-X).
- Hannachi, A., Jolliffe, I.T., Stephenson, D.B., 2007. Empirical orthogonal functions and related techniques in atmospheric science: a review. *Int. J. Climatol.* 27, 1119–1152. <https://doi.org/10.1002/joc.1499>.
- Harris, I., Jones, P.D., Osborn, T.J., Lister, D.H., 2014. Updated high-resolution grids of monthly climatic observations – the CRU TS3.10 dataset. *Int. J. Climatol.* 34, 623–642. <https://doi.org/10.1002/joc.3711>.
- Hoerling, M., Quan, X.-W., Eischeid, J., 2009. Distinct causes for two principal U.S. droughts of the 20th century. *Geophys. Res. Lett.* 36. <https://doi.org/10.1029/2009GL039860>.
- Hossain, F., et al., 2015. Local-to-regional landscape drivers of extreme weather and climate: implications for water infrastructure resilience. *J. Hydrol. Eng.* 20, 02515002. [https://doi.org/10.1061/\(asce\)he.1943-5584.0001210](https://doi.org/10.1061/(asce)he.1943-5584.0001210).
- IPCC, 2014. Summary for Policymakers, 1–30, doi: 10.1017/cbo9781107415324.004.
- Kaiser, H.F., 1958. The varimax criterion for analytic rotation in factor analysis. *Psychometrika* 23, 187–200. <https://doi.org/10.1007/bf02289233>.
- Karl, T.R., Koscielny, A.J., 1982. Drought in the United States: 1895–1981. *J. Climatol.* 2, 313–329. <https://doi.org/10.1002/joc.3370020402>.
- Knapp, A.K., Smith, M.D., 2001. Variation among biomes in temporal dynamics of aboveground primary production. *Science* 291, 481–484. <https://doi.org/10.1126/science.291.5503.481>.
- Köppen, W., 2011. The thermal zones of the Earth according to the duration of hot, moderate and cold periods and to the impact of heat on the organic world. *Meteorologische Zeitschrift* 20, 351–360. <https://doi.org/10.1127/0941-2948/2011/105>.
- Küchler, A.W., 1964. *Potential Natural Vegetation of the Conterminous United States: Map*. American Geographical Society.
- Livneh, B., Hoerling, M.P., 2016. The physics of drought in the U.S. central Great Plains. *J. Clim.* 29, 6783–6804. <https://doi.org/10.1175/JCLI-D-15-0697.1>.
- Logan, K.E., Brunsell, N.A., Jones, A.R., Feddema, J.J., 2010. Assessing spatiotemporal variability of drought in the U.S. central plains. *J. Arid Environ.* 74, 247–255. <https://doi.org/10.1016/j.jaridenv.2009.08.008>.
- Lorenz, E.N., 1956. *Empirical Orthogonal Functions and Statistical Weather Prediction*. Massachusetts Institute of Technology, Department of Meteorology.
- Mann, H.B., 1945. Nonparametric tests against trend. *Econometrica* 13, 245–259. <https://doi.org/10.2307/1907187>.
- Martins, D.S., Razei, T., Paulo, A.A., Pereira, L.S., 2012. Spatial and temporal variability of precipitation and drought in Portugal. *Nat. Hazards Earth Syst. Sci.* 12, 1493–1501. <https://doi.org/10.5194/nhess-12-1493-2012>.
- Massey, F.J., 1951. The Kolmogorov-Smirnov test for goodness of fit. *J. Am. Stat. Assoc.* 46, 68–78. <https://doi.org/10.1080/01621459.1951.10500769>.
- McLeman, R.A., Dupre, J., Berrang Ford, L., Ford, J., Gajewski, K., Marchildon, G., 2014. What we learned from the Dust Bowl: lessons in science, policy, and adaptation. *Popul. Environ.* 35, 417–440. <https://doi.org/10.1007/s11111-013-0190-z>.
- North, K.E., Bell, T.L., Cahalan, R.F., Moeng, F.J., 1982. Sampling errors in the estimation of empirical orthogonal functions. *Mon. Weather Rev.* 110, 699–706. [https://doi.org/10.1175/1520-0493\(1982\)110<0699:seiteo>2.0.co;2](https://doi.org/10.1175/1520-0493(1982)110<0699:seiteo>2.0.co;2).
- Omondi, P., Ogallo, L.A., Anyah, R., Muthama, J.M., Ininda, J., 2013. Linkages between global sea surface temperatures and decadal rainfall variability over Eastern Africa region. *Int. J. Climatol.* 33, 2082–2104. <https://doi.org/10.1002/joc.3578>.
- Overland, J.E., Preisendorfer, R.W., 1982. A significance test for principal components applied to a cyclone climatology. *Mon. Weather Rev.* 110, 1–4. [https://doi.org/10.1175/1520-0493\(1982\)110<0001:astfpc>2.0.co;2](https://doi.org/10.1175/1520-0493(1982)110<0001:astfpc>2.0.co;2).
- Panu, U.S., Sharma, T.C., 2002. Challenges in drought research: some perspectives and future directions. *Hydrol. Sci. J.* 47, S19–S30. <https://doi.org/10.1080/02626660209493019>.
- Peterson, T.C., Karl, T.R., Jamason, P.F., Knight, R., Easterling, D.R., 1998. First difference method: Maximizing station density for the calculation of long-term global temperature change. *J. Geophys. Res.: Atmos.* 103, 25967–25974. <https://doi.org/10.1029/98JD01168>.
- Pielke, R., Doesken, N., 2008. Climate of the short grass steppe in the United States. In: Lauenroth, W.K., Burke, I.C. (Eds.), *Ecology of the Shortgrass Steppe: A Long-Term Perspective*. Oxford University Press.
- Pielke, R.A., Adegoke, J.O., Chase, T.N., Marshall, C.H., Matsui, T., Niyogi, D., 2007. A new paradigm for assessing the role of agriculture in the climate system and in climate change. *Agric. For. Meteorol.* 142, 234–254. <https://doi.org/10.1016/j.agrformet.2006.06.012>.
- Pielke, R.A., Niyogi, D., Adegoke, J., Kallos, G., Seastedt, T.R., Hossain, F., 2013. *Climate Vulnerability: Understanding and Addressing Threats to Essential Resources*. Elsevier/Academic Press.
- Preisendorfer, R.W., Mobley, C.D., 1988. *Principal Component Analysis in Meteorology and Oceanography*. Elsevier.
- Razei, T., Bordini, L., Pereira, L.S., Sutera, A., 2010. Space-time variability of hydrological drought and wetness in Iran using NCEP/NCAR and GPCC datasets. *Hydrol. Earth Syst. Sci.* 14, 1919–1930. <https://doi.org/10.5194/hess-14-1919-2010>.

- Richman, M.B., 1986. Rotation of principal components. *J. Climatol.* 6, 293–335. <https://doi.org/10.1002/joc.3370060305>.
- Russo, T.A., Lall, U., 2017. Depletion and response of deep groundwater to climate-induced pumping variability. *Nat. Geosci.* 10, 105–108. <https://doi.org/10.1038/ngeo2883>.
- Santos, J.F., Pulido-Calvo, I., Portela, M.M., 2010. Spatial and temporal variability of droughts in Portugal. *Water Resour. Res.* 46. <https://doi.org/10.1029/2009WR008071>.
- Sauchyn, D.J., Stroich, J., Beriault, A., 2003. A paleoclimatic context for the drought of 1999–2001 in the northern Great Plains of North America. *Geograph. J.* 169, 158–167. <https://doi.org/10.1111/1475-4959.05003>.
- Shafer, M., et al., 2014. Great Plains. In: Melillo, J.M., Richmond, T.C., Yohe, G.W. (Eds.), *Climate Change Impacts in the United States: The Third National Climate Assessment*. U.S. Global Change Research Program, pp. 441–461. <https://doi.org/10.7930/JOD798BC>. Chapter 19.
- Sönmez, F.K., Kömüscü, A.L.I.Ü., Erkan, A., Turgu, E., 2005. An analysis of spatial and temporal dimension of drought vulnerability in Turkey using the standardized precipitation index. *Nat. Hazards* 35, 243–264. <https://doi.org/10.1007/s11069-004-5704-7>.
- Stockton, C.W., Meko, D.M., 1983. Drought recurrence in the Great Plains as reconstructed from long-term tree-ring records. *J. Climate Appl. Meteorol.* 22, 17–29. [https://doi.org/10.1175/1520-0450\(1983\)022<0017:DRITGP>2.0.CO;2](https://doi.org/10.1175/1520-0450(1983)022<0017:DRITGP>2.0.CO;2).
- Svoboda, M., et al., 2002. The drought monitor. *Bull. Am. Meteorol. Soc.* 83, 1181–1190. [https://doi.org/10.1175/1520-0477\(2002\)083<1181:TDM>2.3.CO;2](https://doi.org/10.1175/1520-0477(2002)083<1181:TDM>2.3.CO;2).
- Tatli, H., Türkes, M., 2011. Empirical Orthogonal Function analysis of the palmer drought indices. *Agric. For. Meteorol.* 151, 981–991. <https://doi.org/10.1016/j.agrformet.2011.03.004>.
- Theil, H., 1950. A rank-invariant method of linear and polynomial regression analysis, 1, 2, and 3. *Ned. Akad. Wetensch Proc.* 53, 386–392.
- Vicente-Serrano, S.M., 2006. Differences in spatial patterns of drought on different time scales: an analysis of the Iberian Peninsula. *Water Resour. Manage.* 20, 37–60. <https://doi.org/10.1007/s11269-006-2974-8>.
- Vicente-Serrano, S.M., Beguería, S., López-Moreno, J.I., 2010. A multiscalar drought index sensitive to global warming: the standardized precipitation evapotranspiration index. *J. Clim.* 23, 1696–1718. <https://doi.org/10.1175/2009jcli2909.1>.
- Vicente-Serrano, S.M., Beguería, S., López-Moreno, J.I., 2011. Comment on “Characteristics and trends in various forms of the Palmer Drought Severity Index (PDSI) during 1900–2008” by Aiguo Dai. *J. Geophys. Res.* 116. <https://doi.org/10.1029/2011jd016410>.
- Villarini, G., Smith, J.A., Vecchi, G.A., 2012. Changing frequency of heavy rainfall over the central United States. *J. Clim.* 26, 351–357. <https://doi.org/10.1175/JCLI-D-12-00043.1>.
- Vose, R.S., et al., 2014. Improved historical temperature and precipitation time series for U.S. climate divisions. *J. Appl. Meteorol. Climatol.* 53, 1232–1251. <https://doi.org/10.1175/JAMC-D-13-0248.1>.
- Wang, K.J., Williams, A.P., Lettenmaier, D.P., 2017. How much have California winters warmed over the last century? *Geophys. Res. Lett.* 44, 8893–8900. <https://doi.org/10.1002/2017GL075002>.
- Wang, S.-Y., Chen, T.-C., 2009. The late-spring maximum of rainfall over the U.S. central plains and the role of the low-level jet. *J. Clim.* 22, 4696–4709. <https://doi.org/10.1175/2009JCLI2719.1>.
- Warwick, R.A., 1975. *Drought Hazard in the United States: A Research Assessment*. I. o. B. S. University of Colorado, Boulder, Colorado.
- Wiener, J.D., Pulwarty, R.S., Ware, D., 2016. Bite without bark: How the socioeconomic context of the 1950s U.S. drought minimized responses to a multiyear extreme climate event. *Weather Clim. Extremes* 11, 80–94. <https://doi.org/10.1016/j.wace.2015.11.007>.
- Wilks, D.S., 2011. *Statistical Methods in the Atmospheric Sciences*, third ed. Academic Press, pp. 676.
- Woodhouse, C.A., Overpeck, J.T., 1998. 2000 years of drought variability in the central United States. *Bull. Am. Meteorol. Soc.* 79, 2693–2714. [https://doi.org/10.1175/1520-0477\(1998\)079<2693:yodvit>2.0.co;2](https://doi.org/10.1175/1520-0477(1998)079<2693:yodvit>2.0.co;2).
- Yuan, S., Quiring, S.M., 2014. Drought in the U.S. Great Plains (1980–2012): a sensitivity study using different methods for estimating potential evapotranspiration in the Palmer Drought Severity Index. *J. Geophys. Res.: Atmos.* 119, 10996–911010. <https://doi.org/10.1002/2014JD021970>.
- Zelen, M., Norman, S., 1964. Probability functions. In: Abramowitz, M., Stegun, I.A. (Eds.), *Handbook of Mathematical Functions: With Formulas, Graphs, and Mathematical Tables*, pp. 933.